https://doi.org/10.36375/prepare_u.iiche.a385

[International Conference on Energy Transition: Challenges and Opportunities at Chemical Engineering Congress (CHEMCON-2023) – On the occasion of Platinum Jubilee Year of Indian Institute of Chemical Engineers]

Biopolymer Supported ZnO Bionanocomposites Film and Their Application in Environmental Remediation and Controlling of Contagious Diseases

Rebika Baruah[a,b*], , Karishma Talukdar[a,b], Vekuno Cukhamu[a], Archana Moni Das[a,b]

[a]*CSIR-North East Institute of Science and Technology, Jorhat-785006, Assam, India*

[b]*Academy of Scientific and Innovative Research (AcSIR), Ghaziabad- 201002, India*

**Corresponding Author's Name: Rebika Baruah,*

Email: baruahrebika9@gmail.com,

Phone number: 9476626581

Abstract

Abstract ID: ANN OP-1
Mention Abstract Theme: Advanced Nano-Materials & Nanotechnology (ANN)

Bionanocomposites are innovative sustainable materials that possess multifunctional attractive nature in various fields. Cellulose/chitosan/ ZnO bionanocomposites (CCZBC) films were synthesized by utilizing water extracts of *Livistona jekinsiana* as reducing as well as capping agents to synthesize ZnO NPs impregnated chitosan/cellulose bionanocomposites thin film. X-ray diffraction pattern of CCZBCC revealed the wurtzite structure of ZnO nanoparticles. Fourier transform infrared spectroscopy revealed the presence of plant extracts, cellulose, and chitosan in CCZBC. Scanning Electron Microscope (SEM) images provided information about the morphology of the surface of CCZBC. The elemental composition of CCZBC was determined by Energy Dispersive X-ray (EDX) analysis. Transmission Electron Microscope (TEM) provided the shape and size of CCZBC. CCZBC possessed efficient photocatalytic degradative properties in the remediation of two anthropogenic dyes, Eosin blue and Bromocresol green, potential antimicrobial activity against *Escherichia coli* (*E. coli*) and *Staphylococcus aureus* (*S. aureus*)., and antioxidant property in DPPH assay. Therefore, the chitosan/cellulose/Ag NPs bionanocomposites film can be considered an efficient material for biomedical and environmental applications.

Keywords: Bionanocomposites; ZnO nanoparticles; Cellulose; Chitosan; Thin Film

1. Introduction

Environmental pollution is a great challenge for human civilization in the 21st century (Khan *et al.* 2018). Water pollution is the main threat to surviving a healthy life in the world (Ahmed *et al.* 2017). Due to the technical evaluation, much wastage is drained off to the water bodies that cause detrimental effects on the aquatic lives (Ahmed *et al.* 2017; Baruah *et al.* 2021). It is an urgent need to develop an innovative and novel technique to remediate water pollutants and make water safe for drinking

(Rashid *et al.* 2021; Baruah *et al.* 2022). Many methods were developed to degrade harmful chemicals in wastewater. Most of them have disadvantages of high pressure, temperature, cost, longer time, larger area, production of byproducts, etc. (Baruah *et al.* 2021). Photocatalysis is the most efficient method that can be applied in wastewater treatment (Rashid *et al.* 2021). This method is a very cost-effective, simple, and eco-friendly method (Vardhan *et al.* 2019; Rashid *et al.* 2021). Photocatalysis in the presence of nanoparticles (NPs) is an ideal alternative to conventional methods (Vardhan *et al.* 2019). Due to the large surface to volume ratio, extra small-size NPs can scavenge organic pollutants within a short period to the larger extent (Goswami *et al.* 2018; Vardhan *et al.* 2019; Liu *et al.* 2019; Rashid *et al.* 2021).

ZnO is an n-type semiconductor belonging to group III-IV family (Baruah *et al.* 2019). ZnO is a universally recognized photocatalyst due to its wide band gap (3.37 eV), high photosensitivity, low cost, and environment-friendly nature (Mishra *et al.,* 2016; Matinise *et al.* 2017; Goswami & Das, 2019; Baruah *et al.* 2023). ZnO efficiently degraded rhodamine B (RhB) (Yadav *et al.* 2018), methyl orange (MO) (Baruah *et al.* 2021), congo red (CR) (Baruah *et al.* 2019), methylene blue (MB) (Baruah *et al.* 2021), and acid red 18 (Kumar *et al.* 2018). Because of its bio-safety, biocompatibility, and biodegradability, it is an important material in pharmaceutical and pro-ecological systems (Stan *et al.* 2015). Therefore, many works have been published in several book reviews and papers regarding the synthesis and application of ZnO. But still, people try to extract the novel character of this promising particle by altering the method of preparation due to its multitasking nature (Varadavenkatesan *et al.* 2019; Golmohammadi *et al.* 2020; Baruah *et al.* 2021).

Synthesis of nanoparticles by green methods is the best solution to the problems arising from the physical and chemical ones (Lu *et al.,* 2019). The interaction of nanoparticles with biomaterials is a demanding area of research (Hassan *et al.* 2015). The green synthesis of nanoparticles includes biologically originated systems. Among them, plants are the most preferable (Fowsiya *et al.* 2016; Singh *et al.* 2019). The secondary metabolites present in the plants act both as reducing and stabilization agents (Rajakumar *et al.* 2018; Agarwal & Shanmugam, 2020; Kamarajan *et al.* 2022). Plants mediated synthesis leads to stable and uniformly shaped and size nanoparticles (Zbair *et al.* 2018; Hadjltaief *et al.*2018; Ong *et al.,* 2018). Many plants are used for the synthesis of nanoparticles like *Livistona jenkinsiana* (Baruah *et al.* 2021), *Alpinia nigra* (Baruah *et al.* 2019), *Hibiscus sabdariffa* (Baruah *et al.* 2023), *Azadirachta indica* (Sharma *et al.* 2021), *Aloe vera* (Sadiq *et al.* 2021), etc.

Phragmites australis is a common reed that belongs to wetland species. The plant is a perennial, widely distributed emergent macrophyte with vigorous growth. It possesses remarkably high amplitude of tolerance. It is the dominant plant species in many watercourses and often forms huge reed beds along many shallow lakes and freshwater canals, especially in Egypt. Phytochemical analysis reveals its abundance of bioactive compounds such as tannins, phenolic compounds, flavonoids, terpenoids, and glycosides (Hosny *et al.,* 2021). These phytochemicals can easily reduce and stabilize the NPs by electrostatic stabilization. This plant

shows potential antibacterial and antioxidant activities (Hosny *et al.*, 2021). *Phragmites australis* mediated Au, Ag, and Cu NPs were reported, but the synthesis of ZnO NPs was reported in this paper for the first time.

In this work, the synthesis of ZnO NPs was carried out using aqueous extracts. *Phragmites australis*. ZnO NPs were characterized by UV-Visible, FTIR, XRD, SEM, TEM, DLS, and zeta potential analysis. Photocatalytic activity of ZnO NPs was screened in the degradation of MO, and MB under solar irradiation. The antibacterial activity of ZnO NPs was studied against *Staphylococcus aureus*, *Escherichia coli, Bacillus subtilis, and Klebsiella pneumonia* by agar well diffusion method. The antioxidant ability of ZnO NPs was also evaluated by using a DPPH scavenging assay.

2. Experimental

2.1. Materials

All the chemicals were used as received without further purification. Chemicals were purchased from Sigma Aldrich and Merk chemicals, Rankem, Himedia, SRL, and LobaChemie. Double-distilled H_2O was used to prepare all the reagent solutions.

2.2. Analytical methods

UV-Vis spectrophotometer (Hitachi Model No –U-3900) was used to observe the characteristics absorption peak of ZnO NPs. FTIR spectroscopy (Perkin-Elmer FT-IR-2000 spectrometer) confirmed the involvement of phytochemicals in the synthesis of ZnO NPs. The crystalline nature and morphology of ZnO NPs were determined by XRD (Rigaku Ultima IV diffractometer) and SEM (ZEISS, SIGMA instrument). Elemental analysis of the NPs was recorded by EDS spectrum. TEM (JEM-2100 Plus) determined the phase, shape, and size of the ZnO NPs. Zeta potential and DLS values were measured by Nano ZS Zetasizer (Malvern) instrument to evaluate the size distribution, polydispersity index (PDI), and electric charge of the nanoparticles. Photocatalytic degradation of MB and MO and scavenging of DPPH by ZnO NPs were examined by a UV-Visible spectrophotometer. The zone of inhibition of harmful pathogens in antibacterial activity was measured using an Antibiotic Zone Scale. Origin Pro 9, Chem Draw 15, and Image J software were used to plot graphs, draw chemical structures, and determine the size of ZnO NPs respectively.

2.3. Preparation of plant extract

Phragmites australis were collected from Holmora Village, North West Jorhat, Assam, India. The plant was washed with double distilled water to remove impurities. Thereafter, the plant was cut into small pieces of 1-2 cm size and dried under sunlight to make them moisture free. Dried small pieces were converted into fine powder by grinding and stored in a zipper bag for further studies.

10 gm of leaves was added to an Erlenmeyer flask containing 100 ml of double distilled. The mixture was treated at 45°C for 60 minutes under stirring. Clear plant extracts were collected by filtration of the mixture followed by centrifugation at 5000 rpm for 30 min. The extract was refrigerated at 4°C for future applications.

2.4. Synthesis of Phragmites australis fabricated ZnO NPs (PA@ZnO NPs)

30 ml of plant extract and 10 mM of $ZnCl_2$ solution were mixed in an Erlenmeyer flask. 10 ml of 1 M NaOH solution was added to the mixture dropwise to make the pH of the mixture 7. Then the mixture was constantly stirred at

https://doi.org/10.36375/prepare_u.iiche.a385

60°C for 3 h to prepare a deep yellow color solution. The formation of PA@ZnO NPs was preliminarily confirmed by observing UV-Vis spectra of ZnO NPs and the color change of the reaction mixture. Then the colloidal solution was sonicated for 1h at 50°C, centrifuged at 6000 rpm for 15 min and washed with 50% C_2H_5OH and H_2O solution. Impurity-free segregated pellets were dried in an oven at 60°C for 12 hours and converted to fine powder form by grinding with mortar and pestle. Obtained PA@ZnO NPs were stored in a vacuum desiccator for different characterization and potent application.

2.5. Photocatalytic activity of the PA@ZnO NPs

Methylene Blue and Methyl Orange were considered as the model dye to examine the photocatalytic activity of PA@ZnO NPs. 2.5 mg of the photocatalyst and 25 ml of each dye solution were mixed (1mg/ml) and kept in dark under stirring conditions for 30 minutes to attain the adsorption-desorption equilibrium. After that, each mixture of dye and NPs was subjected to sunlight under continuous stirring. 2 ml aliquots of each suspension of MB and MO were collected after every 5 minutes and measured the absorption of the mixture at 665 and 463 nm respectively. Thus the time dependant photo degradative effect of the PA@ZnO NPs towards MB and MO dye was examined with the help of a UV-Vis spectrophotometer. The complete degradation of dyes was achieved in 60 minutes.

2.6. Antioxidant activity of PA@ ZnO NPs

DPPH (2, 2-diphenyl-1-picrylhydrazyl) was used as a model free radical in the examination of the antioxidant activity of the PA@ZnO NPs. Ascorbic Acid (AA) and pure DPPH solution were considered as positive and negative standards respectively. Different concentrations (20, 40, 60, 80 & 100µg/ml) of AA and PA@ZnO NPs were prepared in double-distilled water. 1 ml of water was added to each concentration of AA and NPs. 1 ml of DPPH (.1mM of 20 ml ethanolic solution) was also added to them. The prepared solutions were incubated in dark conditions at room temperature for 30 min. The absorbance of each solution was measured at 517 nm against the 30% ethanolic aqueous solution. IC50 value was calculated by plotting the extract concentration on the X-axis versus the corresponding percentage of scavenging effect on the Y-axis in the log dose inhibition curve by using the following formula:

% scavenging = [Absorbance of control - Absorbance of test sample/Absorbance of control] X 100

2.7. Antibacterial activity of PA@ZnO NPs

Bacillus subtilis (MTCC 441) and *Escherichia coli* (ATCC 11229) were selected to screen the antibacterial activity of PA@ZnO NPs by using agar well diffusion method. Fresh bacterial cultures were prepared in Mueller Hinton broth medium, where 10 µl cultures of *E. coli* and *S. aureus* were inoculated separately, and incubated for 18 hours at 37°C, in a shaker until the turbidity resembled with McFarland 0.5 turbidity standard. 100 µl of each pathogen was spread on Petri dishes separately containing sterilized Mueller Hinton agar using a sterilized spreader. Then the wells (6 mm) were made in agar plates by the sterilized well borer and each concentration of PA@ZnO NPs (20, 40, 60, 80, and 100 µg/ml) were added to the respective marked wells and kept at 37°C for 24 h for incubation. The positive control of this experiment was neomycin. The zone of inhibition

https://doi.org/10.36375/prepare_u.iiche.a385

of bacteria was measured in millimeters (mm) by an antibacterial zone measuring scale. The test was performed three times and the results were shown as mean ± standard deviation.

3. Results and Discussions

3.1. UV-Visible spectroscopy

Optical properties of PA@ZnO NPs were studied by UV-Visible spectroscopy in the range of wavelength 200-700 nm. ZnO NPs showed the characteristics absorption peak at 340 nm with the blue shift from the absorption peak of bulk ZnO at 378 nm [Figure 1]. The characteristics absorption peak of ZnO NPs was due to surface Plasmon resonance and the blue shift from the bulk value was due to the quantum confinement effect (Vinayagam *et al.*, 2020). Mie's theory states that one absorption peak reveals the uniform spherical shape of nanoparticles. NPs exhibit more than a single SPR band due to the anisotropicity of the particles. The symmetry of NPs is inversely proportional to the number of SPR (Baruah *et al.* 2021; Baruah *et al.* 2022). Band gap PA@ZnO NPs was calculated by the formula E_g=1240/λ. The band gap was found to be 3.65 eV that value reinforced the semiconducting property of the material. Reported results have similarities with literature like *Livistona jekinsiana* and nanocellulose mediated ZnO NPs showed characteristic absorption peaks at 332 and 368.33 nm respectively (Baruah *et al.* 2021; Baruah *et al.* 2023).

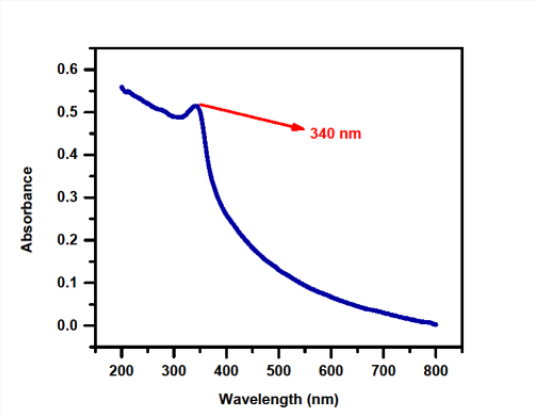

Figure 1: UV-visible spectrum of PA@ZnO NPs.

3.2. FT-IR Analysis

The involvement of phytochemicals in the synthesis and stabilization of PA@ZnO NPs and the chemical composition of ZnO NPs was studied by FTIR analysis [Figure 2]. Different phytoconstituents like phenolic compounds, steroids, flavonoids, terpenoids, alkaloids, etc. are responsible for the fabrication of ZnO NPs (Baruah *et al.* 2019). The band that appeared at 3354 and 2919 cm^{-1} were due to the O–H stretching and the C-H asymmetric and symmetric stretching respectively (Baruah *et al.* 2023). The peak at 1633 cm^{-1} pointed out the –C=C – stretching vibrations of the aromatic compounds (Rajakumar *et al.* 2018). The absorption band at 1470 and 1371 cm^{-1} were due to the C-N stretching vibrations and O-H banding of phenolic compounds (Goswami *et al.* 2018). The absorption band at 888 cm^{-1} was caused by the bending of primary/secondary amines. The sharp band that appeared at 569 cm^{-1} elucidated the stretching vibrations of the Zn-O metallic bond of ZnO NPs (Baruah *et al.* 2021; Baruah *et al.* 2023).

https://doi.org/10.36375/prepare_u.iiche.a385

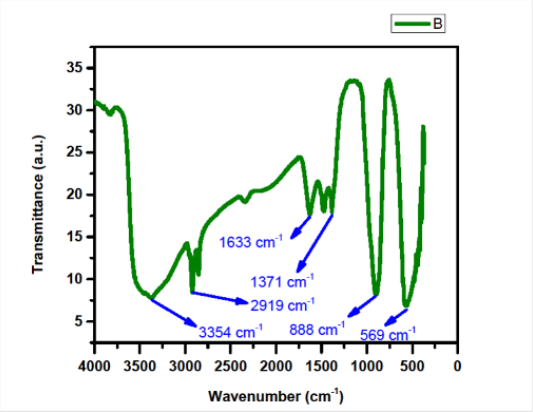

Figure 2: FTIR spectrum of PA@ZnO NPs.

3.3. XRD Analysis

The crystalline nature of PA@ZnO NPs was established by the XRD pattern of ZnO NPs. The characteristic peaks in the plane (100), (002), (101), (102), (110), (103), (112) appeared at 2θ = 31.64°, 34.57°, 36.38°, 47.65°, 56.64°, 62.95°, 67.91° respectively [Figure 3] corresponding with JCPDS (Card Number 36-1451) (Hosny *et al.*, 2021). These peaks revealed the wurtzite structure of ZnO NPs. The comparatively greater peak intensity of the (101) plane was observed which represented preferred growth in the (101) direction (Baruah *et al.* 2021; Baruah *et al.* 2023).

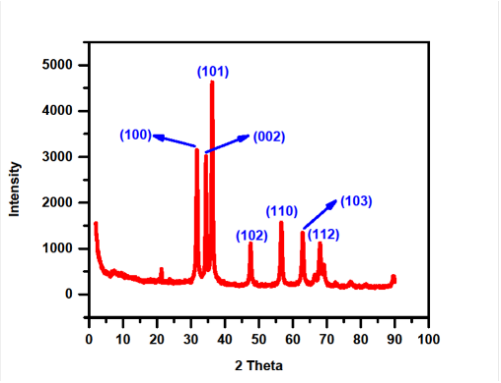

Figure 3: XRD pattern of PA@ZnO NPs.

3.4. FESEM and EDX analysis

Morphology of the surface of PA@ZnO NPs was studied by FESEM of ZnO NPs. SEM images revealed the spherical shape of the ZnO NPs [Figure 4 [A]]. The NPs were uniformly distrusted with lower agglomeration. The agglomeration was due to the high surface energy of ZnO NPs due to the stabilization of biomaterials of the plant extracts.

The elemental composition of PA@ZnO NPs was determined by EDX analysis. The EDX data of ZnO NPs showed signals for Zn and O [Figure 4 [B]], revealing the presence of Zn and O in the ZnO NPs. Other elements C, Cu, Cl, and Si in the EDX spectrum were due to the presence of different phytoconstituents of plant extracts. The SEM and EDX data were in accordance with the literature (Baruah *et al.* 2021; Baruah *et al.* 2023).

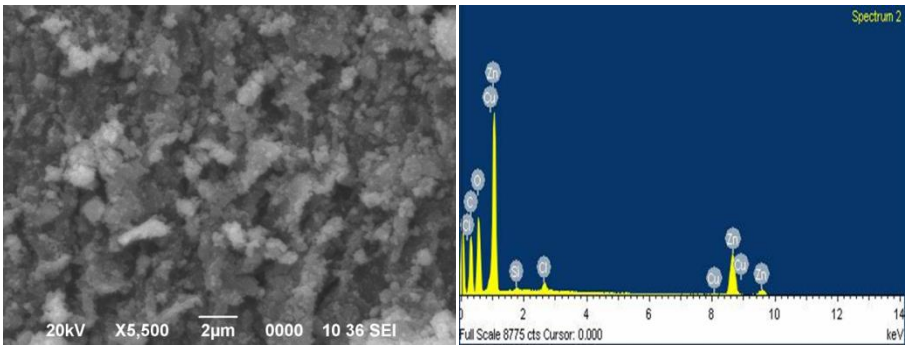

[A] **[B]**

Figure 4: SEM images [A] and EDX spectrum [B] of PA@ZnO NPs.

https://doi.org/10.36375/prepare_u.iiche.a385

3.5. TEM analysis

TEM images of PA@ZnO NPs assigned the shape and size of NPs. The shape of the ZnO NPs was found to be different like spherical, oval, and hexagonal [Figure 5 [A]]. The agglomeration of nanoparticles was observed due to the aqueous medium of the synthesis. The average size of the ZnO NPs was 23 nm with a standard deviation of 2.874 [Figure 5[D]]. The SAED pattern correlated the planes (002), and (110) that the planes resembled the XRD patterns of ZnO NPs [Figure 5 [C]]. The fringe spacing in HRTEM of ZnO NPs was 0.25 nm which corresponded to the (002) plane of the ZnO NPs [Figure 5 [B]]. The TEM results revealed the uniformly dispersed and evenly shaped nature of the ZnO NPs (Baruah *et al.* 2021; Baruah *et al.* 2023).

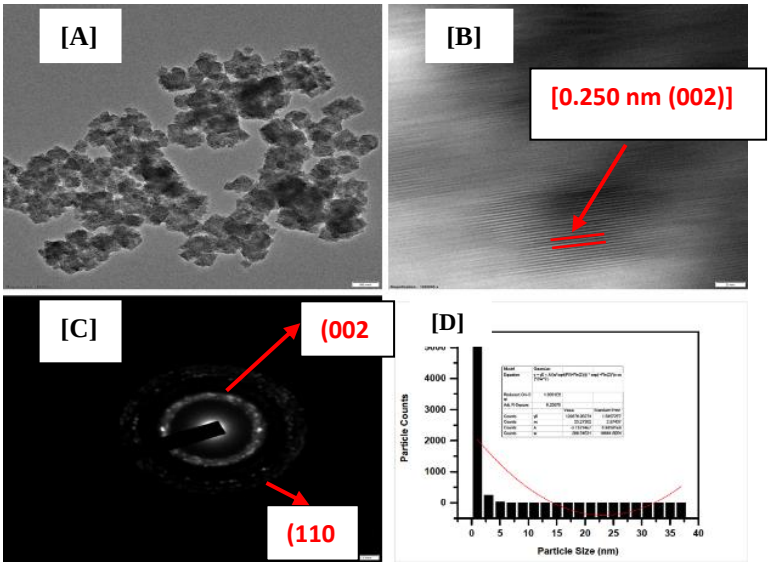

Figure 5: TEM image [A], HRTEM image [B], SAED pattern [C], and average particle size distribution [D] of PA@ZnO NPs.

3.6. Colloidal properties

Zeta potential revealed the colloidal behavior of nanoparticles by providing information about the density of the electric charge on the surface of the particles. The average zeta potential of ZnO NPs was −11.66 mV with a standard deviation of 3.4 [Table 1]. DLVO theory stated that the density of the electric discharge on the surface of the particles is directly proportional to the repulsive force of the static electricity between the particles. This force is responsible for the higher stability of the nanoparticles (Baruah *et al.* 2021; Baruah *et al.* 2023). The reported zeta potential value confirmed that PA@ZnO NPs were stable NPs that were useful for their catalytic application in dye degradation.

DLS analysis determined the hydrodynamic diameter of PA@ZnO NPs and which was in the range of 100-1000 nm [Figure 6]. The hydrodynamic diameter of ZnO NPs was greater that the size of NPs given by TEM analysis due to the solvation effect. The Polydispersity Index (PDI) of ZnO NPs was found to be 0.203 with a standard deviation of 0.894. The results confirmed that the reported eco-friendly method was the successful one to synthesize the stable ZnO NPs.

https://doi.org/10.36375/prepare_u.iiche.a385

Zeta potential and DLS analysis data were similar to the previous literature (Baruah *et al.* 2021; Baruah *et al.* 2023).

Record	Type	Sample Name	T	ZP	Mob	Cond	Wall Zeta Potential
			°C	mV	µmcm/Vs	mS/cm	mV
1	Zeta Potential	PA@ZnO NPs	25	-9.18	-0.7193	199	0
2			25	-12.2	-0.96	205	0
3			25	-13.6	-1.062	206	0

Table 1. Zeta potential of PA@ZnO NPs.

			Size (d.n...	% Intensity:	St Dev (d.n...
Z-Average (d.nm):	1434	**Peak 1:**	587.3	100.0	**76.49**
PdI:	0.720	**Peak 2:**	0.000	0.0	**0.000**
Intercept:	**0.894**	Peak 3:	**0.000**	**0.0**	**0.000**

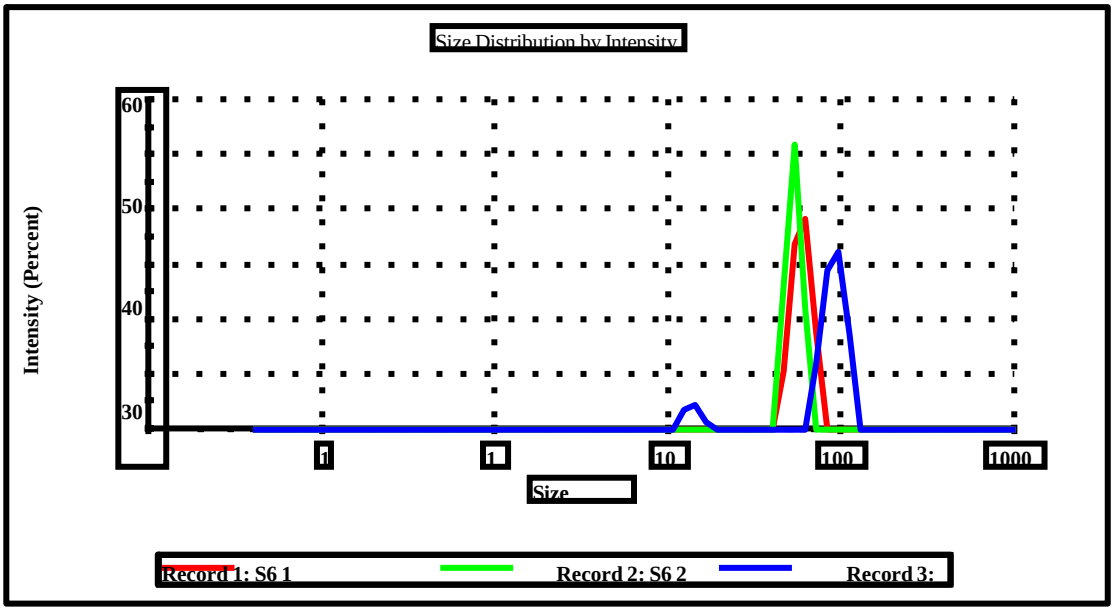

Figure 6: DLS Analysis of PA@ZnO NPs.

3.7. Photocatalytic activity of PA@ZnO NPs

ZnO NPs degraded dye molecules in the presence of photons. Under solar irradiation, the electron (e−) of the valence bond excites to the conduction band and hole (h+) generates in the valance band [eq. (a)]. The hole reacts with adsorbed water molecules and surface-bound hydroxyl groups (OH−) and generates hydroxyl radicals (OH•) [(b) and (c)]. Electron reduces the oxygen molecule present in the solution and produces superoxide radical anion (O2•−) [(d)]. The degradation of MB and MO was proposed to

https://doi.org/10.36375/prepare_u.iiche.a385

take place through a disproportion of the produced free radicals during the reactions [(e)].

The following equations are illustrated to describe the photocatalytic activities of ZnO NPs in the degradation of MB and MO dye:

$$\mathbf{ZnO + h\upsilon \rightarrow e^{-}(CB) + h^{+}(VB)\ (a)}$$

$$\mathbf{h^{+}(VB) + H_2O \rightarrow H^{+} + OH^{\bullet}\ (b)}$$

$$\mathbf{h^{+}(VB) + OH^{-} \rightarrow OH^{\bullet}\ (c)}$$

$$\mathbf{e^{-}(CB) + O2 \rightarrow O2^{\bullet -}\ (d)}$$

$$\mathbf{OH^{\bullet} + O2^{\bullet -} + Dye \rightarrow Degraded\ product\ (e)}$$

3.7.1. Degradation of Methyl Orange and Methylene Blue

PA@ZnO NPs degraded MO in 60 min up to 80% under sunlight. The intensity of the maximum absorption peak of the MO was measured at 463 nm and it was decreased with increasing the irradiation time [Figure 7[A]]. The degradation of MB was also observed in presence of PA@ZnO NPs under solar irradiation. The intensity of the maximum absorption of the MB was measured at 665 nm and decreased with time. Degradation MB was observed for 60 min and the dye degraded up to 82% [Figure 7[B]]. The results were in accordance with the literature. As time proceeded the degradation of the dye increased due to the higher surface energy of PA@ZnO NPs. ZnO NPs degraded harmful dyes to environment-friendly products like H_2O and CO_2 [Figure 8] (Baruah *et al.* 2021; Baruah *et al.* 2023).

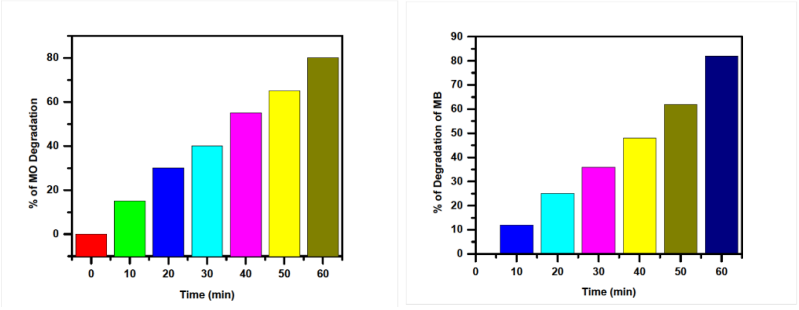

[A] **[B]**

Figure 7: % of Degradation of MO [A] and MB [B].

https://doi.org/10.36375/prepare_u.iiche.a385

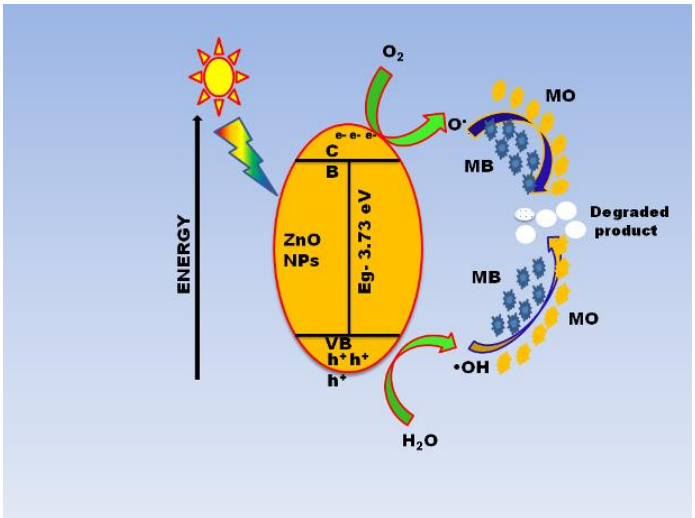

CB – conduction band, VB – Valance band, e^- - electrons, h^+ - holes, $O_2^{-\bullet}$ - superoxide anion radical and •OH – hydroxyl radical

Figure 8: Mechanism of Photodegradation effect of PA@ZnO NPs under solar irradiation.

3.8. Biomedical application of PA@ZNO NPs

3.8.1. Antioxidant activity

The antioxidant activity of PA@ZnO NPs was studied by considering DPPH as a model free radical. Characteristics maximum absorption peak of this radical at 517 nm decreased with the increasing concentration of ZnO NPs. The purple-colored DPPH reacts with an antioxidant in the presence of a hydrogen donor and becomes paired off yellow-colored DPPHH (Stan *et al.* 2015). The IC50 value AA and ZnO NPs were found to be 60.00 and 85.05µg/ml respectively [Figure 9]. Due to the high surface area to volume ratio, ZnO NPs efficiently interacted with DPPH and reduced it (Baruah *et al.* 2021; Baruah *et al.* 2023). IC50 values have resembled literature. Therefore, it is possible to propose an Equation below:

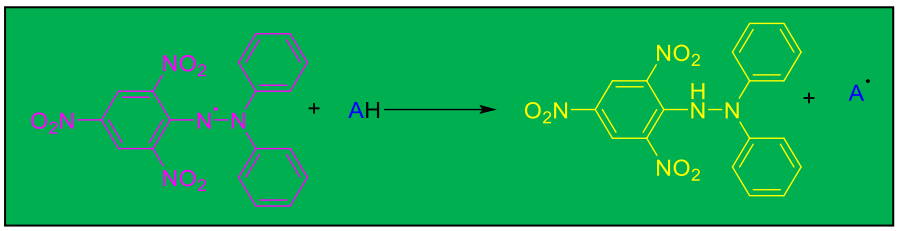

DPPH **DPPHH**

https://doi.org/10.36375/prepare_u.iiche.a385

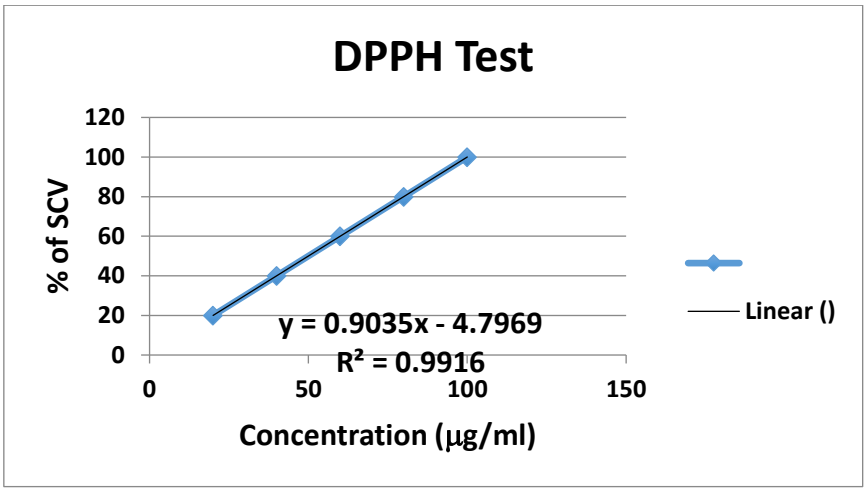

[A]

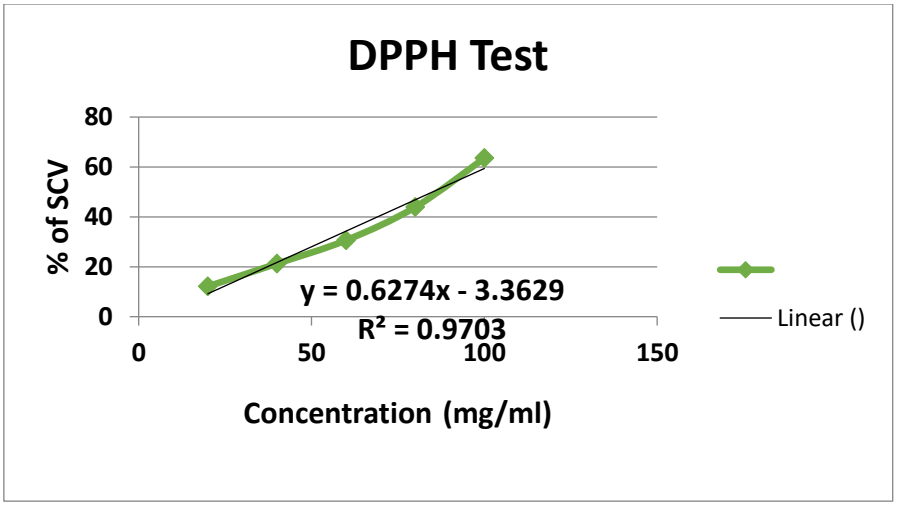

[B]

Figure 9: Antioxidant activity of Ascorbic acid [A], and PA@ZnO NPs [B].

3.8.2. Antimicrobial activity of PA@ZnO NPs

PA@ZnO NPs were applied against gram-positive *S. aureus* and gram-negative *E. coli* and they behaves as broad-spectrum antibiotics. The diameter of the inhibition zone was listed in Table 2. The zone of inhibition (mm) against *S. aureus* measured 10 ± 0.50, 12 ± 0.20, 14 ± 0.40, and 16 ± 0.10; against *E. coli* measured 9 ± 0.40, 10 ± 0.70, 11 ± 0.30, and 13 ± 0.40 mm; for concentrations at 30, 60, 90 and 120 µg/ml, respectively. The inhibition zone of bacteria increased as the concentration of ZnO NPs increased [Fig. 10]. ZnO NPs could more efficiently inhibit the growth of gram-positive bacteria than that of gram-negative ones. The different structural components of the cell wall of both bacteria are the reason for this selectivity. The cell wall of gram-positive bacteria is composed of peptidoglycan (80%). Teichoic acids and proteins and lipopolysaccharide compose the other portion of the cell wall and outer membrane respectively. The cell wall of gram-negative bacteria is composed of only 10% peptidoglycan and the outer membrane contains 50% lipopolysaccharides, 35% phospholipids, and 15%

https://doi.org/10.36375/prepare_u.iiche.a385

lipoproteins and gives resistance to the bacteria towards antibiotics (Baruah *et al.* 2021; Baruah *et al.* 2022). The results were similar to literature (Baruah *et al.* 2023).

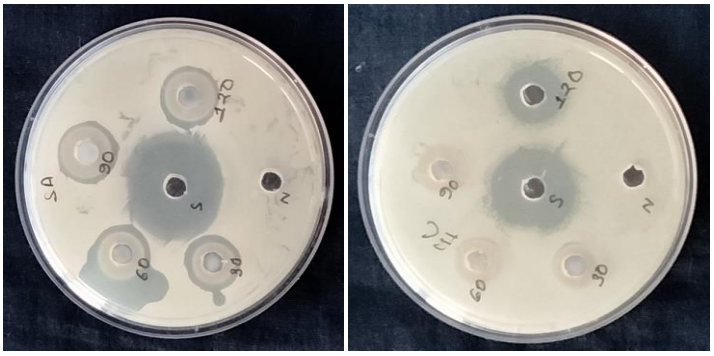

[A] **[B]**

Figure 10: Inhibition zone of *S. aureus* [A], and *E. coli.* [B] in presence of PA@ZnO NPs.

S No.	Test Organisms	Zone of Inhibition (in mm) for different concentrations of ZnO NPs				Neomycin (Standard) (ZI)[b]
		1	2	3	4	
11	*S. aureus*	10± 0.50	12± 0.20	14± 0.40	16± 0.10	26± 0.50
22	*E. coli*	9± 0.40	10± 0.70	11± 0. 30	13± 0.40	22± 0.60

Table 2. Diameter of inhibition zone (in mm) of tested bacteria in the presence of PA@ZnO NPs

4. Conclusion

Phragmites australis fabricated ZnO NPs were synthesized via a mild and simple method for the first time. The contribution of phytochemicals in the synthesis and stabilization of PA@ZnO NPs was confirmed by the FTIR spectrum. The characteristics absorption peak of ZnO NPs appeared at 340 nm in the UV-visible spectrum due to the SPR of ZnO NPs. The hexagonal wurtzite structure of ZnO NPs was confirmed by the XRD pattern of NPs. SEM and TEM images determined the morphology, shape, and size of the ZnO NPs and the size of the nanoparticles was 23 nm with a standard deviation of 2.874. The stability of the nanoparticles was determined by zeta potential with a value of −11.66 mV with a standard deviation of 3.4. The size, size distribution, and polydispersity index of the nanoparticles were analyzed by DLS value that was in the range of 100-1000 nm. EDS provides information on the elemental composition and purity of ZnO NPs. PA@ZnO NPs efficiently photocatalyzed the degradation of MO and MB under solar irradiation up to 80% and 82% respectively. ZnO NPs showed broad-spectrum antibiotics against *S. aureus* and *E. coli*. ZnO NPs also showed potent antioxidant activity with an IC50 value of 85.05 μg/ml. Hence,

Phragmites australis fabricated ZnO NPs is a new efficient, and environmentally friendly candidate to overwhelm water pollution and infectious diseases.

Acknowledgments

The authors were sincerely grateful to the Director of CSIR-North East Institute of Science and Technology, Jorhat, Assam for his valuable guidance to perform our research with excellent facilities. R. B. acknowledged the Department of Science and Technology, New Delhi, for the Fellowship grants.

Conflict of Interest: There is no conflict of interest

References

[1] Khan, S. A., Noreen, F., Kanwalc, S., Iqbal, A., & Hussain, G. (2028). Green synthesis of ZnO and Cu-doped ZnO nanoparticles from leaf extracts of *Abutilon indicum, Clerodendrum infortunatum, Clerodendrum inerme* and investigation of their biological and photocatalytic activities. *Materials Science & Engineering: C, 82,* 46–59. https://doi.org/10.1016/j.msec.2017.08.071

[2] Ahmed, S., Chaudhry, S. A., & Ikram, S. (2017). A review on biogenic synthesis of ZnO nanoparticles using plant extracts and microbes: A prospect towards green chemistry. *Journal of Photochemistry and Photobiology B: Biology, 166,* 272-284. https://doi.org/10.1016/j.jphotobiol.2016.12.011

[3] Baruah, R., Yadav, A., & Das, A. M. (2021). *Livistona jekinsiana* fabricated ZnO nanoparticles and their detrimental effect towards anthropogenic organic pollutants and human pathogenic bacteria. *Spectrochimica Acta Part A: Molecular and Biomolecular Spectroscopy, 251,* 119459. https://doi.org/10.1016/j.saa.2021.119459

[4] Baruah, R., Yadav, A., & Das, A. M. (2022). Evaluation of the multifunctional activity of silver bionanocomposites in environmental remediation and inhibition of the growth of multidrug-resistant pathogens†. *New Journal of Chemistry, 46,* 10128-10153. 10.1039/D1NJ06198D

[5] Vardhan, K. H., Kumar, P. S., & Panda, R. C. (2019). A review on heavy metal pollution, toxicity and remedial measures: Current trends and future perspectives. *Journal of Molecular Liquids, 290,* 111197. https://doi.org/10.1016/j.molliq.2019.111197

[6] Rashid, T., Sherf, F., Hazafa, A., Hashmi, R. Q., Zafar, A., Rasheed, T., & Hussain, S. (2021). Design and feasibility study of novel paraboloid graphite based microbial fuel cell for bioelectrogenesis and pharmaceutical wastewater treatment. *Journal of Environmental Chemical Engineering, 9 (1),* 104502. https://doi.org/10.1016/j.jece.2020.104502

[7] Liu, Y., Zhang, Q., Xu, M., Yuan, H., Chen, Y., Zhang, J., Luo, K., Zhang, J., & You, B. (2019). Novel and efficient synthesis of Ag-ZnO nanoparticles for the sunlight-induced photocatalytic degradation. *Applied Surface Science, 476,* 632–640. https://doi.org/10.1016/j.apsusc.2019.01.137

[8] Goswami, M., Baruah, D., & Das, A. M. (2018). Green synthesis of silver nanoparticles supported on cellulose and their catalytic application in the scavenging of organic dyes. *New Journal of Chemistry, 42,* 10868-10878. 10.1039/C8NJ00526E

[9] Baruah, D., Yadav, R.N.S., Yadav, A., & Das, A.M. (2019). *Alpinia nigra* fruits mediated synthesis of silver nanoparticles and their antimicrobial and photocatalytic activities. *Journal of Photochemistry & Photobiology B: Biology, 201,* 111649.

https://doi.org/10.1016/j.jphotobiol.2019.111649

[10] Goswami, M. & Das, A. M. (2019). Synthesis and Characterization of a Biodegradable Cellulose Acetate-Montmorillonite Composite for Effective Adsorption of Eosin Y. *Carbohydrate Polymers, 206,* 863-872. https://doi.org/10.1016/j.carbpol.2018.11.040

[11] Mishra, P., Singh, Y. P., Nagaswarupa, H. P., Sharma, S. C., Vidya, Y. S., Prashantha, S. C., Nagabhushana, H., Anantharaju, K. S., Sharma, S., & Renuka, L. (2016). *Caralluma fimbriata* extract induced green synthesis, structural, optical and photocatalytic properties of ZnO nanostructure modified with Gd. *Journal of Alloys and Compounds, 685,* 656-669. https://doi.org/10.1016/j.jallcom.2016.05.044

[12] Matinise, N., Fuku, X. G., Kaviyarasu, K., Mayedwa, N., & Maaza, M. (2017). ZnO nanoparticles via *Moringa oleifera* green synthesis: physical properties & mechanism of formation. *Applied Surface Science, 406,* 339-347. https://doi.org/10.1016/j.apsusc.2017.01.219

[13] Baruah, R., Goswami, M., Das, A. M., Nath, D., & Talukdar, K. (2023). Multifunctional ZnO Bionanocomposites in the Treatment of Polluted Water and Controlling of Multi-drug Resistant Bacteria. *Journal of Molecular Structure, 1283,* 35251. https://doi.org/10.1016/j.molstruc.2023.135251

[14] Yadav, L. S. R., Raghavendra, M., Manjunath, K., & Nagaraju, G. (2018). Photocatalytic, biodiesel, electrochemical sensing properties and formylation reactions of ZnO nanoparticles synthesized via eco-friendly green synthesis method. *Journal of Materials Science: Materials in Electronics, 29,* 8747-8759. https://doi.org/10.1007/s10854-018-8891-9

[15] Kumar, K. H. S., Dhananjaya, N., & Yadav, L. S. R. (2018). *E. Tirucalli* plant latex mediated green combustion synthesis of ZnO nanoparticles: structure, photoluminescence and photo-catalytic activities. *Journal of Science: Advanced Materials and Devices, 3(3),* 303-309. https://doi.org/10.1016/j.jsamd.2018.07.005

[16] Stan, M., Popa, A., Toloman, D., Dehelean, A., Lung, I., & Katona, G. (2015). Enhanced Photocatalytic Degradation Properties of Zinc Oxide Nanoparticles Synthesized by Using Plant Extracts. *Materials Science in Semiconductor Processing, 39,* 23-29. https://doi.org/10.1016/j.mssp.2015.04.038

[17] Varadavenkatesan, T., Lyubchik, E., Pai, S., Pugazhendhi, A., Vinayagam, R., & Selvaraj, R. (2019). Photocatalytic Degradation of Rhodamine B by Zinc Oxide Nanoparticles Synthesized Using the Leaf Extract of Cyanometra Ramiflora. *Journal of Photochemistry and Photobiology B: Biology, 199,* 111621. https://doi.org/10.1016/j.jphotobiol.2019.111621

[18] Golmohammadi, M., Honarmand, M., & Ghanbari, S. (2020). A Green Approach to Synthesis of ZnO Nanoparticles Using Jujube Fruit Extract and Their Application in Photocatalytic Degradation of Organic Dyes. *Spectrochimica Acta Part A: Molecular and Biomolecular Spectroscopy, 229,* 117961. https://doi.org/10.1016/j.saa.2019.117961

[19] Lu, J., Batjikh, I., Hurh, J., Han, Y., Ali, H., Mathiyalagan, R., Ling, C., Ahn, J. C., & Yang, D. C. (2019). Photocatalytic Degradation of Methylene Blue Using Biosynthesized Zinc Oxide Nanoparticles from Bark Extract of Kalopanax Septemlobus. *Optik, 182,* 980-985. https://doi.org/10.1016/j.ijleo.2018.12.016

[20] Hassan, S. S. M., Azab, W. I. M. E., Ali, H. R., & Mansour, M. S. M. (2015). Green Synthesis and Characterization of ZnO

Nanoparticles for Photocatalytic Degradation of Anthracene. *Advances in Natural Sciences: Nanoscience and Nanotechnology, 6(4),* 045012. 10.1088/2043-6262/6/4/045012

[21] Singh, K., Singh, J., Rawat, M., Green Synthesis of Zinc Oxide Nanoparticles Using Punica Granatum Leaf Extract and Its Application towards Photocatalytic Degradation of Coomassie Brilliant Blue R-250 Dye. *SN Applied Sciences, 1,* 1-8. https://doi.org/10.1007/s42452-019-0610-5

[22] Fowsiya, J., Madhumitha, G., Al-Dhabi, N. A., & Arasu, M. V. (2016). Photocatalytic Degradation of Congo Red Using Carissa Edulis Extract Capped Zinc Oxide Nanoparticles. *Journal of Photochemistry and Photobiology B: Biology, 162,* 395-401. https://doi.org/10.1016/j.jphotobiol.2016.07.011

[23] Kamarajan, G., Anburaj, D. B., Porkalai, V., Muthuvel, A., & Nedunchezhian, G. (2022). Green Synthesis of ZnO Nanoparticles Using Acalypha Indica Leaf Extract and Their Photocatalyst Degradation and Antibacterial Activity. Journal of the Indian Chemical Society, 99, 100695. https://doi.org/10.1016/j.jics.2022.100695

[24] Rajakumar, G., Thiruvengadam, M., Mydhili, G., Gomathi, T., & Chung, I. M. (2018). Green approach for synthesis of zinc oxide nanoparticles from *Andrographis paniculata* leaf extract and evaluation of their antioxidant, anti-diabetic, and anti-inflammatory activities. *Bioprocess and Biosystems Engineering, 41,* 21-30. https://doi.org/10.1007/s00449-017-1840-9

[25] Agarwal, H., & Shanmugam, V. K. (2020). A review on anti-inflammatory activity of green synthesized zinc oxide nanoparticle: Mechanism-based approach. Bioorganic Chemistry, 94, 103423. https://doi.org/10.1016/j.bioorg.2019.103423

[26] Zbair, M., Anfar, Z., Ait Ahsaine, H., Alem, N. E., & Ezahri, M. (2018). Acridine orange adsorption by zinc oxide/almond shell activated carbon composite: Operational factors, mechanism and performance optimization using central composite design and surface modeling. Journal of Environmental Management, 206, 383-397. https://doi.org/10.1016/j.jenvman.2017.10.058

[27] Hadjltaief, H. B., Ameur, S. B., Costa, P. D. Zina, M. B., & Galvez, M. E. (2018). Photocatalytic decolorization of cationic and anionic dyes over ZnO nanoparticle immobilized on natural Tunisian clay. *Applied Clay Science, 152,* 148-157. https://doi.org/10.1016/j.clay.2017.11.008

[28] Ong, C. B., Ng, L. Y., & Mohammad, A. W. (2018). A Review of ZnO Nanoparticles as Solar Photocatalysts: Synthesis, Mechanisms and Applications. Renewable and Sustainable Energy Reviews, 81, 536-55. https://doi.org/10.1016/j.rser.2017.08.020

[29] Sharma, J. L., Dhayal, V., & Sharma, R. K. (2021). White-rot fungus mediated green synthesis of zinc oxide nanoparticles and their impregnation on cellulose to develop environmental friendly antimicrobial fibers. *3 Biotech, 11,* 269. https://doi.org/10.1007/s13205-021-02840-6

[30] Sadiq, H., Sher, F., Sehar, S., Lima, E. C., Zhang, S., Iqbal, H. M. N., Zafar, F., & Nuhanović, M. (2021). Green Synthesis of ZnO Nanoparticles from Syzygium Cumini Leaves Extract with Robust Photocatalysis Applications. *Journal of Molecular Liquids, 335,* 116567. https://doi.org/10.1016/j.molliq.2021.116567

[31] Hosny, M., Fawzy, M., El-Borady, O. M., & Mahmoud, A. E. D. (2021). Comparative study between Phragmites australis root and rhizome extracts for mediating gold nanoparticles synthesis and their medical and environmental applications. *Advanced Powder*

Technology, *32*, 2268-2279. https://doi.org/10.1016/j.apt.2021.05.004

[32] Vinayagam, R., Selvaraj, R., Pugazhendhi, A., & Varadavenkatesan, T. (2020). Synthesis, characterization and photocatalytic dye degradation capability of Calliandra haematocephala-mediated zinc oxide nanoflowers, Journal of Photochemistry & Photobiology, B: Biology, 203, 111760. https://doi.org/10.1016/j.jphotobiol.2019.111760